Yu, S., et al., 2023, Evolutionary history of the groundwater system in the Pearl River Delta (China) during the Holocene: Geology, https://doi.org/10.1130/G50888.1

# Supplemental Material

# Evolutionary history of groundwater system in the Pearl River Delta during the Holocene

Shengchao Yu[1,2], Jiu Jimmy Jiao[1,3,*], Xin Luo[1,3], Hailong Li[2], Xuejing Wang[4], Xiaolang Zhang[1,2], Meng Yao[2], Jinchao Zuo[2], Wenzhao Liang[1], Meiqing Lu[1,2]

[1] Department of Earth Sciences, The University of Hong Kong, Hong Kong.

[2] School of Environmental Science and Engineering, Southern University of Science and Technology, Shenzhen, China.

[3] Southern Marine Science and Engineering Guangdong Laboratory (Zhuhai), Zhuhai, China

[4] Institute of Surface-Earth System Science, School of Earth System Science, Tianjin University, Tianjin, China

[*] Corresponding author: J. Jiao (jjiao@hku.hk)

## Quaternary delta systems under the Holocene transgression

Previous hydrogeological investigations have been conducted in worldwide Quaternary deltas which were impacted during the Holocene transgression and regression. The paleo-saltwater from Holocene transgression can be enriched or diluted due to the buffering and filtering effects of deltaic aquifer systems and the fluctuant paleo precipitation. Results show that the intrusion distance of paleo saltwater ranges from several kilometers to hundreds of kilometers and most of which are below two hundred kilometers, and the groundwater salinity varies from brackish to brine.

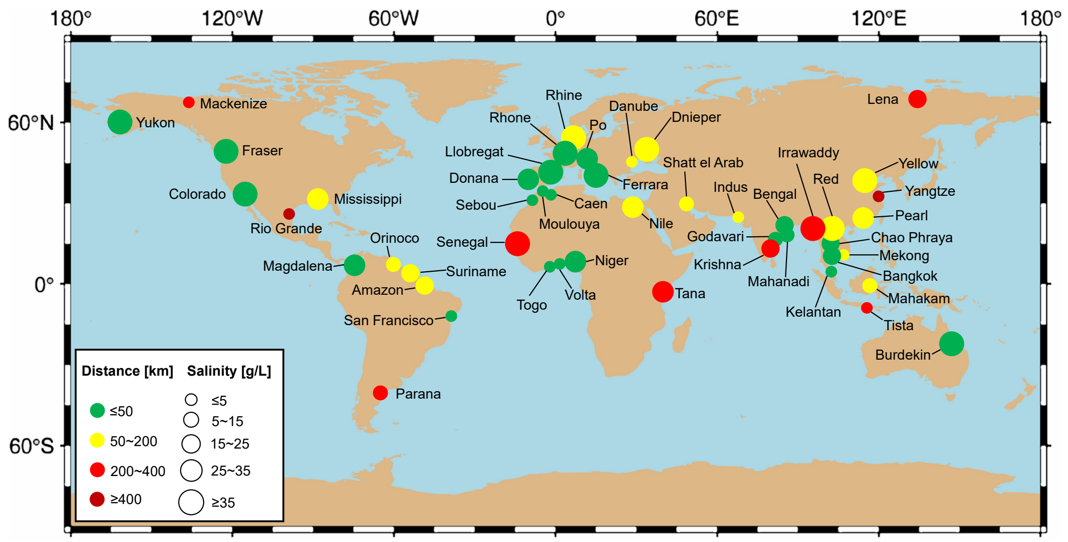


Figure S1. Locations of the 50 deltas with information on saltwater intrusion distance and salinity, whose detailed data can be found in Table S1.

Table S1. Quaternary delta systems in which paleo-saltwater has been reported.

| **Delta** | **Continent** | **Distance km** | **Max salinity g/L** | **Reference** |
|---|---|---|---|---|
| Amazon | South America | 100 | 23 | Bernardino et al., 2022 |
| Bangkok | Asia | 30 | 22 | Das, 1985 |
| Bengal | Asia | 40 | 21 | Sherin et al., 2020 |
| Burdekin | Oceania | 5 | 35 | Narayan et al., 2007 |
| Caen | Europe | 10 | 1.2 | Barbecot et al., 2000 |
| Chao Phraya | Asia | 25 | 17.5 | Eslami et al., 2021 |
| Colorado | North America | 30 | 39 | Smith et al., 1999 |
| Danube | Europe | 60 | 0.4 | Oosterberg et al., 2000 |
| Dniepr | Asia | 120 | 35 | Naudts et al., 2006; Stovba and Stephenson, 2000 |
| Donana | Europe | 18 | 30 | Manzano et al., 2001 |
| Ebro | Europe | 25 | 14.5 | Albert and Jorge,1998 |
| Ferrara | Europe | 14 | 200 | Giambastiani et al., 2013 |
| Fraser | North America | 7 | 43 | Simpson and Hutcheon, 2013 |
| Godavari | Asia | 40 | 12 | Bobba, 2002 |
| Grijalva | North America | 46 | 33 | Alcérreca-Huerta et al., 2019; Cardoso-Mohedano et al., 2022 |
| Red | Asia | 75 | 39 | Tran et al., 2012 |
| Indus | Asia | 60 | 2 | Eslami et al., 2021 |
| Irrawaddy | Asia | 280 | 35 | Rodolfo, 1975 |
| Kelantan | Asia | 6 | 7.2 | Samsudin et al., 2008 |

| | | | | |
|---|---|---|---|---|
| Krishna | Asia | 360 | 18 | Kannan et al., 2022 |
| Lena | Asia | 250 | 17.5 | Bolshiyanov et al., 2015 |
| Llobregat | Europe | 12 | 39 | Manzano et al., 2001 |
| Mackenzie | North America | 200 | 0.15 | Kipp et al., 2020 |
| Magdalena | South America | 6 | 30 | Restrepo et al., 2016 |
| Mahakam | Oceania | 100 | 6 | Storms et al., 2005; Collins et al., 2020 |
| Mahanadi | Asia | 17 | 11.4 | Radhakrishna, 2001 |
| Mekong | Asia | 80 | 2 | Eslami et al., 2021 |
| Mississippi | North America | 60 | 30 | Shiller and Boyle, 1991; Törnqvist etal., 2020 |
| Moulouya | Africa | 40 | 1 | Shaghude, 2005 |
| Niger | Africa | 40 | 30 | Kashef, 1983 |
| Nile | Africa | 60 | 26 | Geriesh et al., 2015 |
| Orinoco | South America | 100 | 9 | Echezuría et al., 2022 |
| Parana | South America | 300 | 10 | Baigún et al., 2008 |
| Po | Europe | 10 | 30 | Cencini, 1998; Pellizzari et al., 2009 |
| Rhine | Europe | 120 | 39 | Post et al., 2003 |
| Rhone | Europe | 23 | 38 | De Montety et al., 2008 |
| Rio Grande | North America | 1200 | 3 | Witcher et al., 2004 |
| Sao Francisco | South America | 20 | 2 | Andrews et al., 2017 |
| Sebou | Africa | 35 | 0.5 | Haddout et al., 2007 |
| Senegal | Africa | 300 | 85 | Barbiero et al., 2001 |
| Shatt el Arab | Asia | 92 | 8 | Abdullah et al., 2016; Al-Jawad et al., 2018 |
| Suriname | South America | 57 | 24 | Groen et al., 2000 |
| Tana | Africa | 250 | 32 | Bouillon et al., 2007; Mutia et al., 2021 |
| Tista | Asia | 300 | 1 | Afroza et al., 2009 |
| Togo | Africa | 25 | 0.4 | Akouvi et al., 2008 |
| Volta | Europe | 33 | 2 | Addo et al., 2018 |
| Yangtze | Asia | 640 | 3 | Dai et al., 2011 |
| Yellow | Asia | 100 | 48 | Yu et al., 2014; Zhang et al., 2017 |
| Yukon | North America | 32 | 40 | Harris, 1990; Terenzi et al., 2014 |
| Zhujiang | Asia | 60 | 28 | Wang and Jiao, 2012 |

## The geology and hydrogeology of the PRD

There was a rapid sea-level rise between 10000 and 7000 years before the present (yr BP) and then the rate slowed down, and the sedimentation switched from transgressive to regressive with rapid shoreline advancing (Zong et al., 2006, 2009a, 2009b). Given the importance of historically changing surface boundaries in shaping the current distribution of groundwater salinity, the stratigraphic accumulation and shoreline migration induced by the sea-level change were implemented by successive time slices, in order to reconstruct the evolution of the aquifer-aquitard system in the Holocene. The $^{13}C$ data from cores in the PRD suggested a strong freshwater flux in the middle Holocene, and from 6000 to 1000 yr BP the weather was relatively wet but became progressively drier in the last 1000 years (Zong, 2004; Zong et al., 2006). Evidence revealed that precipitation had reduced progressively in the late Holocene (Zong et al., 2006), indicating that if current precipitation was used for the simulation in the entire Holocene the freshwater flux by rainfall recharge would be significantly underestimated. The salinity of the paleo seawater near the PRD was lower than the current seawater during most of the Holocene probably due to higher precipitation based on the information of diatom assemblages from borehole cores as water salinity indicators for coastal environments (Zong et al., 2010a, 2010b). A borehole with the most salinity data over the longest period shows that overall the salinity was 30‰ at ~8550 yr BP, decreased to the lowest salinity of ~20‰ around 5000 yr BP, and increased gradually to ~30‰ in the last 1000 years (Zong et al., 2010b).

## Fieldwork and laboratory analysis

Six geological boreholes in three representative field sites were drilled along the northwest-southeast transect in Pearl River Delta. The borehole cores were delivered to Sun Yat-Sen University to study stratigraphy, and some samples were delivered to the State Key Laboratory of Estuarine and Coastal Research, East China Normal University for AMS $^{14}C$ dating. The geological and dating information can be found in Fig. S2 and Table S2. After the borehole was drilled, both permanent multilevel groundwater sampling system and groundwater level monitoring system at each site were installed. Then the flushing of sampling and monitoring systems was immediately performed to avoid the blockage of the sampling points. Groundwater was sampled regularly using a peristaltic pump (Solinst, Co). The in-situ sampling from this multilevel groundwater sampling system, in contrast to porewater squeezing from borehole cores or surface geophysical measurement, provides the most direct and active information for groundwater salinity distribution in the Quaternary delta system.

Monthly sampling was conducted between July 2021 and June 2022. A volume of 50 mL porewater was filtered through 0.45 μm filters and collected in Nalgene tubes for major ion and stable isotope analyses. The portable multi-parameter water quality analyzer (HI9829T, HANA) was used to measure the chemical and physical parameters such as temperature, pH, oxidation-reduction potential (ORP), dissolved oxygen (DO), electrical conductivity (EC), total dissolved solids (TDS), and salinity. The cations ($Na^+$, $K^+$, $Ca^{2+}$, $Mg^{2+}$) and anions ($CI^-$, $SO_4^{2-}$) were analyzed using Ionic Chromatography (Thermo Scientific Dionex ICS-1100) and Inductively Coupled Plasma Optical Emission Spectrometer respectively in the Hydrogeology Lab of Department of Earth Sciences, The University of Hong Kong. Concentrations of dissolved ammonium, nitrate and nitrate, and orthophosphate were measured using Flow Injection Analyzer (Lachat Instruments Quickchem 8000) within one week of sampling at the Southern University of Science and Technology. Errors of nutrient analysis are <10% for $NH_4^+$, <3% for $NO_3^-$ and $NO_2^-$, and <5% for $PO_4^{3+}$. The total alkalinity was in-situ measured by titrating the groundwater samples (~100 mL) with 0.16 N or 1.6 N $H_2SO_4$ solution (Boyd, 2015). The dissolved inorganic carbon, $HCO_3^-$, and $CO_3^{2-}$ were calculated based on the total alkalinity, pH, salinity, and temperature data using the CO2SYS program (Cao et al., 2011; Lewis and Wallace, 1998). Stable isotopes were measured by Isotope Ratio Mass Spectrometry (Thermo Scientific 253 Plus, Germany) at the Southern University of Science and Technology. The $\delta^2H$ and $\delta^{18}O$ values were reported relative to the Vienna Standard Mean Ocean Water (VSMOW). The measurement uncertainties of $\delta^2H$ and $\delta^{18}O$ were 0.6% and 0.1%, respectively.

## Geological information from boreholes

The geological information of drilled boreholes was shown in Fig. S2. The representative boreholes in the Pearl River Delta used to build the numerical model were shown in Table. S2. The aquifer-aquitard system can be constructed based on the geologic description and $^{14}C$ dating results. Twenty-layer samplers were arranged in each permanent multilevel groundwater sampling system and the sampling depths can be seen in Table. S3. Whether the groundwater samples can be collected was decided by the hydraulic conductivity, porosity and specific storage in different layers, and there are 8, 10, and 14 desirable samples in sampling systems SD, HP and MZ, respectively (Fig. S2).

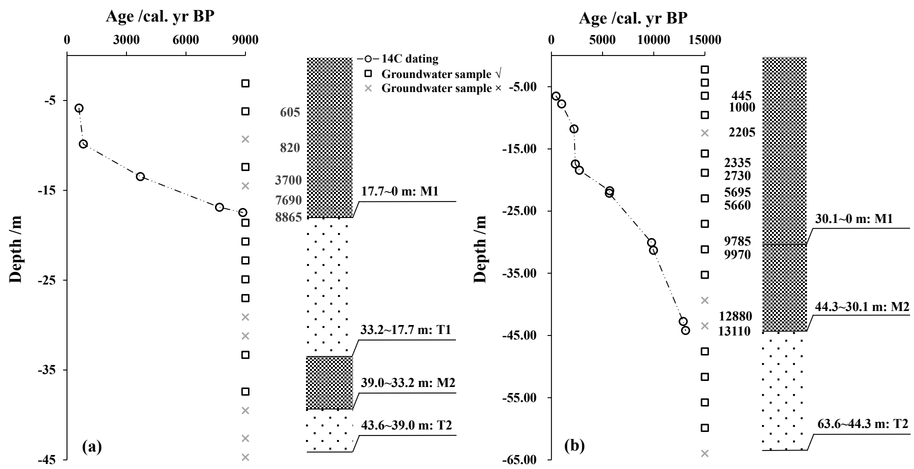


Figure S2. Geological profiles of Cores HP (a) and MZ (b) respectively. The left number means the $^{14}C$ dating result and the right means the depth boundary between the aquifer-aquitard system.

Table S2. Description of the 6 representative sediment cores. The two terrestrial sequences in the Pearl River deltaic basin were named the T1 and T2 units, and the two marine sequences, the M1 and M2 units.

| Depth (m) | Altitude (m. MSL) | Description | Unit |
|---|---|---|---|
| Core K4 (Alt. 3.0 m of mean sea level, N23°11’44”, E112°36’12”) | | | |
| 14C dating: calibrated age of 40.6–37.9 ka BP at depth of 9.3 m | | | |
| 0.0-0.9 | +3.0 ~ +2.1 | Soil | M1 |
| 0.9-6.5 | +2.0 ~ -3.5 | Yellowish grey silt and fine sands | T1 |
| 6.5-9.1 | -3.5 ~ -6.1 | Yellowish red silt and clay (weathered layer) | M2 |
| 9.1-12.5 | -6.1 ~ -9.5 | Yellowish grey fine sands | |
| 12.5-18.3 | -9.5 ~ -15.3 | Coarse sands and gravel | T2 |
| 18.3- | | Bedrock | |
| Core HJ1 (Alt. 1.0 m of mean sea level, N23°05’18”, E113°55’13”) | | | |
| 0.0-0.5 | +1.0 ~ +0.5 | Soil | M1 |
| 0.5-5.5 | +0.5 ~ -4.5 | Yellowish grey fine sands and silt | |
| 5.5-9.8 | -4.5 ~ -8.8 | Dark grey silt and clay | |
| 9.8-20.1 | -8.8 ~ -19.1 | Yellowish grey coarse sands | T1 |
| 20.1-24.5 | -19.1 ~ -23.5 | Grey silt and clay | M2 |
| 24.5-26.8 | -23.5 ~ -25.8 | Yellowish fine sands | T2 |
| 26.8-30.6 | -25.8 ~ -29.6 | Coarse sands and gravel | |
| 30.6- | | Bedrock | |
| Core PK25 (Alt. 1.0 m of mean sea level, N22°57’13”, E113°03’48”) | | | |
| 14C dating: calibrated age of 8.8-8.4 ka BP at depth of 12.6 m | | | |
| 0.0-0.4 | +1.0 ~ +0.6 | Soil | M1 |
| 0.4-2.7 | +0.6 ~ -1.7 | Yellowish grey fine sands and silt | |
| 2.7-12.6 | -1.7 ~ -11.6 | Dark grey silt and clay | |
| 12.6-17.4 | -11.6 ~ -16.4 | Yellowish grey coarse sands | T1 |
| 17.4-20.9 | -16.4 ~ -19.9 | Yellowish red silt and clay (weathered layer) | |
| 20.9-33.8 | -19.9 ~ -32.8 | Grey silt and clay | M2 |
| 33.8-36.9 | -32.8 ~ -35.9 | Coarse sands and gravel | T2 |
| 36.9- | | Bedrock | |
| Core ZK83 (Alt. 1.0 m of mean sea level, N22°55’00”, E113°12’39”) | | | |
| 14C dating: calibrated age of 7.7-7.4 ka BP at depth of 13 m | | | |
| 0.0-0.4 | +1.0 ~ +0.6 | Soil | M1 |
| 0.4-2.3 | +0.6 ~ -1.3 | Yellowish fine sands | |
| 2.3-11.8 | -1.3 ~ -10.8 | Dark grey silt and clay | |
| 11.8-15.8 | -10.8 ~ -14.8 | Grey silt and clay | |
| 15.8-21.2 | -14.8 ~ -20.2 | Yellow coarse sands | T1 |

| | | | |
|---|---|---|---|
| 21.2-34.1 | -20.2 ~ -33.1 | Grey silt and clay | M2 |
| 34.1-35.8 | -33.1 ~ -34.8 | Yellowish grey fine sands | T2 |
| 35.8-39.8 | -34.8 ~ -38.8 | Coarse sands and gravel | |
| 39.8- | | Bedrock | |
| Core HP (Alt. 1.0 m of mean sea level, N22°44’04”, E113°25’50”) | | | |
| 14C dating: calibrated age of 3.9-3.5 ka BP at depth of 13.5 m | | | |
| 14C dating: calibrated age of 7.9-7.5 ka BP at depth of 16.9 m | | | |
| 14C dating: calibrated age of 9.0-8.6 ka BP at depth of 17.5 m | | | |
| 0.0-5.1 | +1.0 ~ -4.1 | Grey silt | M1 |
| 5.1-11.2 | -4.1 ~ -10.2 | Grey silt and clay | |
| 11.2-11.8 | -10.2 ~ -10.8 | Grey silt and clay | |
| 11.8-14.1 | -10.8 ~ -13.1 | Grey silt | |
| 14.1-16.4 | -13.1 ~ -15.4 | Grey silt | |
| 16.4-17.7 | -15.4 ~ -16.7 | Grey silt and clay | |
| 17.7-33.2 | -16.7 ~ -32.2 | Yellow coarse sands | T1 |
| 33.2-39.0 | -32.2 ~ -38.0 | Grey silt and clay | M2 |
| 39.0-43.6 | -38.0 ~ -42.6 | Yellowish grey fine sands | T2 |
| 43.6- | | Bedrock | |
| Core MZ (Alt. -0.5 m of mean sea level, N22°38’21”, E113°32’06”) | | | |
| 14C dating: calibrated age of 2.9-2.5 ka BP at depth of 18.4 m | | | |
| 14C dating: calibrated age of 5.8-5.5 ka BP at depth of 21.7 m | | | |
| 14C dating: calibrated age of 9.9-9.6 ka BP at depth of 30.1 m | | | |
| 14C dating: calibrated age of 13.0-12.8 ka BP at depth of 42.7 m | | | |
| 14C dating: calibrated age of 13.2-11.1 ka BP at depth of 44.2 m | | | |
| 0.0-7.0 | -0.47 ~ -7.5 | Grey silt | M1 |
| 7.0-11.0 | -7.5 ~ -11.5 | Grey silt and clay | |
| 11.0-18.2 | -11.5 ~ -18.7 | Grey silt | |
| 18.2-30.1 | -18.7 ~ -30.6 | Grey silt | |
| 30.1-44.3 | -30.6 ~ -44.8 | Grey silt and clay | M2 |
| 44.3-63.6 | -44.8 ~ -64.1 | Yellow coarse sands | T2 |
| 63.6- | | Bedrock | |

Table S3. The sampling depths of twenty-layer samplers in each permanent multilevel groundwater sampling system.

| Layer No. | Sampling field SD | Sampling field HP | Sampling field MZ |
|---|---|---|---|
| 1 | -0.4 | -3.1 | -2.3 |
| 2 | -1.5 | -6.2 | -4.2 |
| 3 | -3.1 | -9.3 | 6.3 |
| 4 | -4.7 | -12.4 | -9.4 |

| | | | |
|---|---|---|---|
| 5 | -6.3 | -14.5 | -12.5 |
| 6 | -7.9 | -18.6 | -15.6 |
| 7 | -9.0 | -20.7 | -18.7 |
| 8 | -10.1 | -22.8 | -22.8 |
| 9 | -11.2 | -24.9 | -26.9 |
| 10 | -11.8 | -27.0 | -31.0 |
| 11 | -12.4 | -29.1 | -35.3 |
| 12 | -14.5 | -31.2 | -39.4 |
| 13 | -15.6 | -33.3 | -43.5 |
| 14 | -16.7 | -37.4 | -47.6 |
| 15 | -18.8 | -39.5 | -51.7 |
| 16 | -20.9 | -42.6 | -55.8 |
| 17 | -23.0 | -44.7 | -59.9 |
| 18 | -25.1 | -47.8 | -64.0 |
| 19 | -28.2 | -50.9 | -68.1 |
| 20 | -37.3 | -54.0 | -78.2 |

## Groundwater flow and solute transport modeling

The governing equations for groundwater flow, solute transport, and groundwater age in the two-dimensional vertical cross-section perpendicular to the coastline can be written as (Bethke and Johnson, 2002, 2008; Geng and Boufadel, 2015; Jiang et al., 2012; Mao et al., 2023; Xie et al., 2022):

$$\beta\phi\frac{\partial S}{\partial t}+\beta S_0 S\frac{\partial \psi}{\partial t}+\phi S\frac{\partial \beta}{\partial t}=\frac{\partial}{\partial x}\left(\beta\delta k_r K_x\frac{\partial \psi}{\partial x}\right)+\frac{\partial}{\partial z}\left[\beta\delta k_r K_z\left(\frac{\partial \psi}{\partial z}+\beta\right)\right] \tag{S1}$$

$$\phi S\frac{\partial c}{\partial t}=\beta\,\nabla\cdot(\mathbf{D}\nabla c)-\mathbf{q}\cdot\nabla c \tag{S2}$$

$$\phi S\frac{\partial \tau}{\partial t}=\phi S\,\nabla\cdot(\mathbf{D}\,\nabla\tau)-\mathbf{q}\cdot\nabla\tau+\phi S\cdot 1 \tag{S3}$$

where $\beta$ is the density ratio [-], $\varepsilon$ is a fitting parameter and equals $7.143\times10^{-4}$ $m^3/kg$, $c$ is the groundwater salinity [$ML^{-3}$]; $S_0$ is the specific storage [$L^{-1}$], $\psi$ is the groundwater pressure head [L], $t$ is time [T], $\phi$ is the porosity of the porous medium [-], $x$ and $z$ are the horizontal and vertical spatial coordinates [L] of the two-dimensional cross-section domain, with the positive direction of $z$ being upward and the positive direction of $x$ being seaward; the parameter $\delta$ is the dynamic viscosity ratio [-], $K_x$ and $K_z$ are the horizontal and vertical hydraulic conductivity for saturated freshwater [$LT^{-1}$], $\mathbf{D}$ represents the hydrodynamic dispersion tensor, $\mathbf{q}$ is the Darcy velocity [$LT^{-1}$], $\tau$ is the groundwater age, $S$ is water saturation.

The 182 km long transect is extended to the inland watershed boundary to include a complete groundwater system. The thickness of the aquifer-aquitard system above the bedrock ranges from 4 m to almost 60 m. The model domain was divided into 38 layers and represented by 911 columns. Each column was 200 m wide. The thicknesses of the layers increase from 0.02 m in the surface layer to 2.76 m in the basal aquifer with the maximum depth. The small thickness near the surface was chosen to accommodate the small sedimentation rate of deposition at the top boundary.

We assumed the no-flow boundaries (groundwater divides and hydrogeological base) on the inland and bottom sides. On the seaward boundary, the Dirichlet boundary condition was applied. The pressure head was determined by the changing sea level and the salt boundary condition here was determined by the flow direction. When the water flowed into the aquifer a Dirichlet boundary condition was applied at the constant seawater salinity. On the contrary, when water was leaving the aquifer a zero dispersive flux boundary condition was employed. Since the paleo-precipitation has reduced progressively in the late Holocene, the changing recharge from the top boundary and changing infiltration area due to rapid shoreline advancing were applied. In order to conduct the self-regulating setup for rainfall infiltration, the seepage face boundary condition was applied on the top boundary. The upper boundary moved as the sea level changed but was fixed during each time slice, while the boundary conditions changed at each time step, such as the precipitation recharge, sea level and salinity in seawater (Fig. S3).

The pre-Holocene sea level was far below the present level as well as the bottom Quaternary strata in the model, and this relation lasted for tens of thousands of years (Waelbroeck et al., 2002). Hence, it was assumed that the groundwater system in the modeled area was entirely fresh at the beginning of the simulation, so the initial salinity in Pleistocene units was set as zero. The simulated results (head and solute concentration) at the end of each time slice were used as the initial conditions for the next time slice (Delsman et al., 2014), and the elements were added to the model to represent the sedimentation or expansion of the model as a result of transgression at a time slice. The newly added elements at that time were given a concentration of seawater in the seaward direction and given a concentration of freshwater in the inland, respectively. The change of the Quaternary delta system during the Holocene was implemented using six sequential time slices as shown in Table S4.

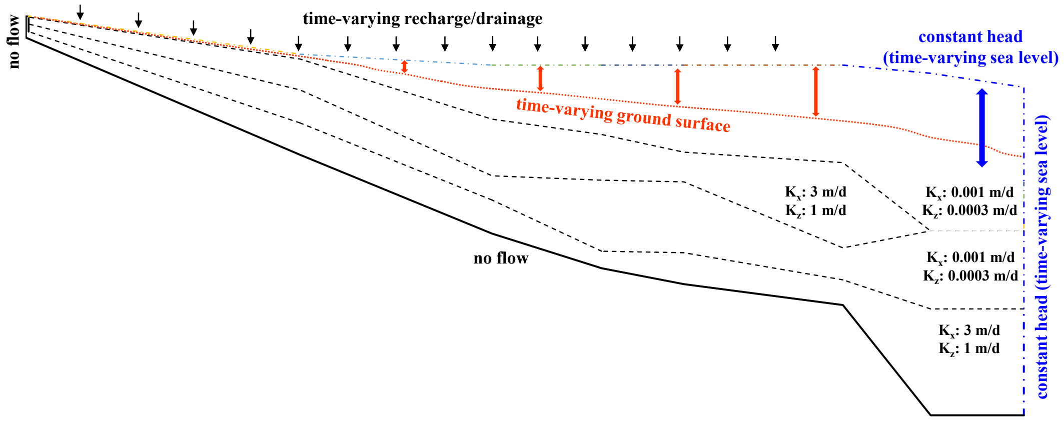


Figure S3. Model setup and boundary conditions.

Table S4. Description of model time slices.

| Time slice | Description |
|---|---|
| 10 ka BP~8 ka BP | Sea level rose linearly from -52 to -25 m; initial transgression; sedimentation rate ranged from 1.83~2.52 mm/yr. |
| 8 ka BP~6 ka BP | Sea level rose linearly from -25 to -2 m; maximum transgression extent occurred; sedimentation rate ranged from 1.83~2.52 mm/yr; an increase in freshwater flux; salinity decreased from 30‰ with a rate of 0.003‰/yr. |
| 6 ka BP~5 ka BP | Sea level fluctuated at -3.17 m; first regression development with freshening of hinterland; sedimentation rate ranged from 1.40~2.52 mm/yr; relatively wet weather but progressively drier; salinity decreased at a rate of 0.003‰/yr. |
| 5 ka BP~3 ka BP | Sea level fluctuated at -2.98 m; regression development accelerated, deltaic progradation rate at 17 m per year; sedimentation rate ranged from 1.11~2.26 mm/yr; relatively wet weather but progressively drier; salinity increased from 20‰ with a rate of 0.001‰/yr. |
| 3 ka BP~0.3 ka BP | Sea level fluctuated at -2.01 m; regression development with 15 m per year deltaic progradation rate; sedimentation rate ranged from 1.82~5.31 mm/yr; progressively reduced precipitation; salinity increased at a rate of 0.001‰/yr. |
| 0.3 ka BP~ current | Sea level fluctuated at -2.01 m; maximal regression development; current precipitation; salinity increased at a rate of 0.001‰/yr. |

We supposed the initial conditions of groundwater age would have no impact on the final results after Holocene transgression and regression, and hence the initial conditions of age in the model domain were set as zero. On the top boundary, the recharge from rainfall can be regarded the freshwater with the age boundary condition set as zero. The age boundary condition in the seaward direction was determined by the flow-direction. When the water flowed into the aquifer a Dirichlet boundary condition was applied with the zero age of inflow seawater. On the contrary, when water was leaving the aquifer a zero dispersive flux boundary condition ($\partial\tau / \partial t = 0$) was employed.

The nutrient boundary was set as the interaction between anoxic groundwater and oxic seawater. Infiltrating seawater provided salinity, dissolved oxygen, dissolved organic matter, bicarbonate and ammonium, and the landward groundwater was assigned as the source of nitrate and metal element. The modelling of biogeochemical processes in the coastal deltaic system was conducted by using the reaction network comprised of kinetic reactions, including heterotrophic/autotrophic denitrification, nitrification, anaerobic ammonium oxidation, redox of iron, and decomposition of dissolved organic carbon due to aerobic respiration, as shown in Table S5. The boundary concentrations at the different endmembers for each species are given in Table S6. The bottom seawater in the Pearl River Estuary was selected as the seawater endmember. The salinity has experienced some changes during the Holocene, and hence the variations of other solutes in the seawater endmember during the Holocene can be decided based on their ratios to salinity. The synchronous changes of salinity and nutrient level can be supported by carbon isotopic records of corals (Su et al., 2014), and dynamics of primary productivity in the South China Sea (Devendra et al., 2019; Zhang et al., 2016). The boundary concentrations at the freshwater endmember were determined as the lowest ones in our observed groundwater samples and were treated as constants during the Holocene. The precipitation was assumed to provide the freshwater with zero solute concentration.

Table S5**.** Reaction network used in the model. Reaction parameter values used in the model was referred to Spiteri et al. (2008a, 2008b; 2008c).

| Name | Reaction | Reaction rate |
| --- | --- | --- |
| Oxic degradation | $DOC + O_2 + HCO_3^- \rightarrow$ <br> $CO_2 + NH_4^+ + HPO_4^{2-} + H_2O$ | If $O_2 > kmo2, R = k_{fox}[DOC]$; <br> If $O_2 < kmo2, R = k_{fox}[DOC][O_2])/kmo2$. |
| Heterotrophic denitrification | $DOC + NO_3^- \rightarrow$ <br> $N_2 + CO_2 + HCO_3^- + NH_4^+ + HPO_4^{2-} + H_2O$ | If $O_2 > kmo2, R = 0$; <br> If $O_2 < kmo2$ and $NO_3 > kmno3, R = k_{fox}[DOC](1-[O_2]/kmo2)$; <br> If $O_2 < kmo2$ and $NO_3 < kmno3, R = k_{fox}[DOC](1-[O_2]/kmo2)([NO_3]/kmno3)$. |
| Autotrophic denitrification | $FeS_2 + NO_3^- + H_2O \rightarrow$ <br> $Fe(OH)_3 + SO_4^{2-} + N_2 + H^+$ | If $O_2 > kmo2, R = 0$; <br> If $O_2 < kmo2$ and $NO_3 > kmno3, R = k_{pydenit}[NO_3](1-[O_2]/kmo2)$; <br> If $O_2 < kmo2$ and $NO_3 < kmno3, R = k_{pydenit}[NO_3](1-[O_2]/kmo2)([NO_3]/kmno3)$. |
| Nitrification | $NH_4^+ + O_2 + HCO_3^- \rightarrow NO_3^- + CO_2 + H_2O$ | $R=k_{nitri}[NH_4][O_2]$ |
| Anaerobic ammonium oxidation | $NH_4^+ + NO_2^- \rightarrow N_2 + H_2O$ | If $O_2 > kmo2, R = 0$; <br> If $O_2 < kmo2$ and $NO_2 > kmno2, R = k_{anammox}[NO_2](1-[O_2]/kmo2)$; <br> If $O_2 < kmo2$ and $NO_2 < kmno2, R = k_{anammox}[NO_2](1-[O_2]/kmo2)([NO_2]/kmno2)$. |
| $Fe(OH)_3$ reduction | $DOC + Fe(OH)_3 + CO_2 \rightarrow$ <br> $Fe^{2+} + HCO_3^- + NH_4^+ + HPO_4^{2-}$ | If $NO_3 > kmno3, R = 0$; <br> If $NO_3 < kmno3$ and $Fe(OH)_3 > kmfe, R = k_{fox}[DOC](1-[O_2]/kmo2-[NO_3]/kmno3)$; <br> If $NO_3 < kmno3$ and $Fe(OH)_3 < kmfe, R = k_{fox}[DOC](1-[O_2]/kmo2-[NO_3]/kmno3)([Fe(OH)_3]/kmfe)$. |
| $Fe^{2+}$ oxidation | $Fe^{2+} + O_2 + HCO_3^- + H_2O \rightarrow Fe(OH)_3 + CO_2$ | $R = k_{feox}[Fe^{2+}][O_2]$ |

Model parameters and their values used in simulations can be seen in Table S7. The first half of the parameters were calibrated when simulating the groundwater flow and salt distribution. After that, their values were fixed, and the second half of the parameters, i.e. the reaction parameter values, were calibrated again when simulating the nutrient transport and reaction. During these processes, the effect of flow rate on kinetic reaction and the determination of the endmembers were major sources of uncertainty for the solute species analysis (Michael et al., 2011; Spiteri et al., 2008b). To consider how this uncertainty may affect the results, we performed the sensitivity analyses (Table S6) around the base case parameter set to assess the effects of freshwater flux by precipitation and solute concentrations for each species in different endmembers on nutrient distributions and fluxes across the sediment-water interface. The base case selected the averaged solute concentrations of the seawater endmember and the lowest ones at the freshwater endmember, then the lowest and highest solute concentrations of the seawater endmember and the averaged and highest solute concentrations of the freshwater endmember were used for sensitivity analyses.

Table S6. Sensitivity analyses of freshwater flux and solute concentrations for each species in different endmembers. * denotes as the base case.

| Variables | Values |
|---|---|
| Rainfall infiltration (m/day) | $9.68\times10^{-7}$*, $1.14\times10^{-6}$, $8.36\times10^{-7}$ |
| $Cl^-$ (mM) | 535* |
| DOC (mM) | 6.8*, 4.25, 9.25 |
| $HCO_3^-$ (mM) | 29.2*, 21.0, 32.0 |
| $NH_4^+$ (mM) | 10.1*, 7.0, 11.6 |
| $O_2$ (mM) | 0.27*, 0.25, 0.28 |
| $Fe^{2+}$ (mM) | 0.04*, 0.05, 0.09 |
| $NO_3^-$ (mM) | 0.10*, 0.11, 0.14 |

Table S7. Model parameters and their values used in simulations. Reaction parameter values used in the model were referred to Spiteri et al. (2008a, 2008b; 2008c).

| Parameter | Description | Value |
|---|---|---|
| $K_{x1}$, m day$^{-1}$ | horizontal hydraulic conductivity of aquitards | 0.001 |
| $K_{x2}$, m day$^{-1}$ | horizontal hydraulic conductivity of aquifers | 3 |
| $K_{z1}$, m day$^{-1}$ | vertical hydraulic conductivity of aquitards | 0.0003 |
| $K_{z2}$, m day$^{-1}$ | vertical hydraulic conductivity of aquifers | 1 |
| $\varphi_1$, - | porosity of aquitards | 0.3 |
| $\varphi_2$, - | porosity of aquifers | 0.4 |
| $S_s$, m$^{-1}$ | specific storage | $1.0\times10^{-5}$ |
| $S_r$, - | residual soil saturation | 0.05 |

| | | |
|---|---|---|
| $\alpha$, $m^{-1}$ | capillary fringe parameter | 5 |
| $n$, - | sand grain size distribution | 4 |
| $\alpha_L$, m | longitudinal dispersivity | 50.5 |
| $\alpha_T$, m | transverse dispersivity | 5.05 |
| $k_{fox}$, $s^{-1}$ | rate constant for DOC decomposition | $3.0\times10^{-9}$ |
| $k_{pydenit}$, $s^{-1}$ | rate constant for denitrification | $2.2\times10^{-8}$ |
| $k_{nitri}$, $mM^{-1}$ $s^{-1}$ | rate constant for nitrification | $4.8\times10^{-4}$ |
| $k_{anammox}$, $mM^{-1}$ $s^{-1}$ | rate constant for anaerobic ammonium oxidation | $6.8\times10^{-7}$ |
| $k_{feox}$, $mM^{-1}$ $s^{-1}$ | rate constant for $Fe^{2+}$ oxidation | $6.4\times10^{-2}$ |
| $kmo2$, mM | limiting concentration of $O_2$ | 0.008 |
| $kmno3$, mM | limiting concentration of $NO_3^-$ | 0.001 |
| $kmfe$, mM | limiting concentration of $Fe(OH)_3$ | 18.95 |

# Model calibration

Cores HP and MZ have been picked to construct our simulation model. Hence, the observed salinity and other chemical concentrations of groundwater samples collected in the permanent multilevel groundwater sampling systems HP and MZ can be applied to calibrate our model. The calibration results can be seen in Figs. S4 and S5. Results showed that our model, after the calibrations of groundwater flow dynamic and solute transport, produced the reliable distribution of age tracers (Fig. S6), showing a good correlation between simulated groundwater age and measured groundwater age. We have measured the ages of groundwater samples in this area based on radiocarbon dating (Wang and Jiao, 2012), and the observed data was used here. All of the groundwater in the deltaic aquifer-aquitard system had been refreshed during the Holocene transgression and regression with the groundwater age less than 10,000 years, also showing that the initial conditions of groundwater age had no impact on the final results in our Holocene-scale model.

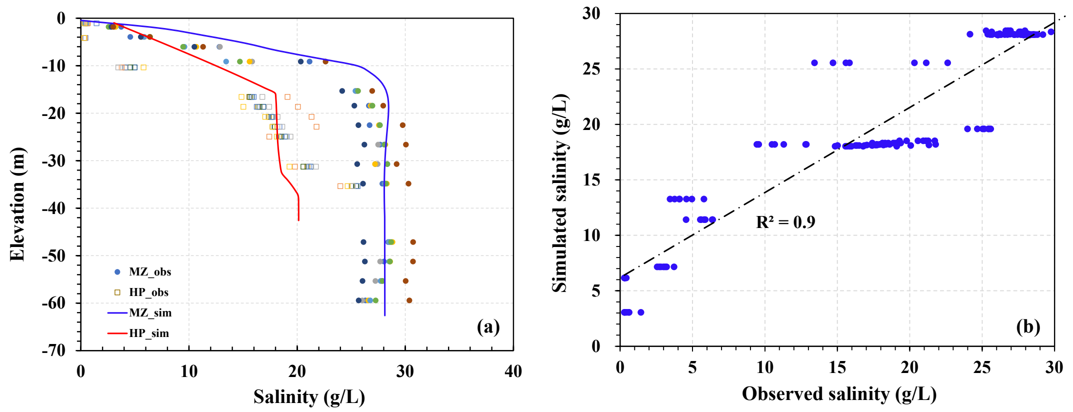


Figure S4. (a) Observed salinity profiles during various seasons and simulated salinity profiles in sampling systems HP and MZ. (b) Correlations between the observed and simulated salinities.

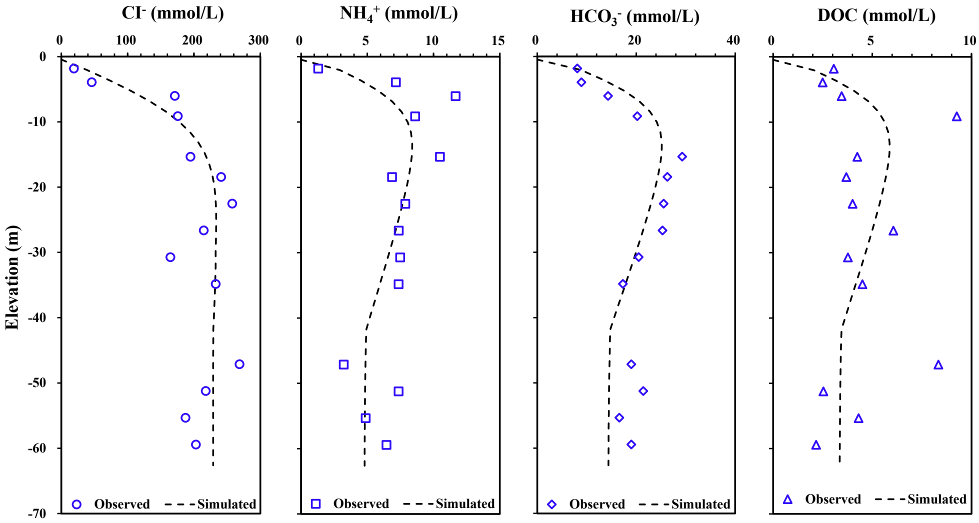


Figure S5. Observed and simulated profiles of chloride, ammonium, bicarbonate and dissolved organic carbon in site MZ.

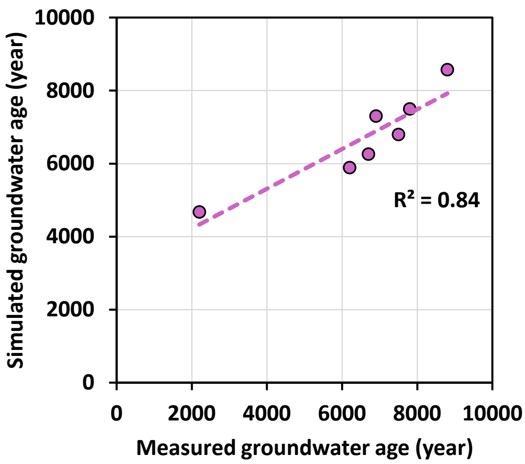


Figure S6. The comparison between simulated groundwater age and measured groundwater age based on radiocarbon dating.

# Results

Fig. S7 shows the evolutionary history of groundwater salinity and transit time in the Quaternary delta system during the Holocene. Under the lower sea level in the late Pleistocene, the inland fresh groundwater flowed across the entire delta system and the whole of deltaic aquifer systems was full of fresh groundwater. During the early Holocene transgression about 8000 yr BP when the sea level started to rise at the right boundary, the saltwater intruded laterally near the bottom of the aquifer. The fresh groundwater flowed through the basal aquifer with a short transit time due to the topographic gradient (Figs. S7a and S7g), and then came across the intruded saltwater. Due to the fast groundwater exchange here, the saltwater flowed upward into the shallow aquifer and aquitard and eventually flowed back to the sea. When the sea level dramatically rose in the severe Holocene transgression, the seawater directly inundated the Quaternary delta system and thereby the typical aquifer-aquitard system emerged in the submerged deltaic sediment. That is, the groundwater transit time in the shallow and basal aquifers was less than that in the aquitards (Fig. S7h). After that, the typical deltaic aquifer-aquitard system gradually developed in the inland direction with a rapid shoreline advancing (Figs. S7i-S7l).

In Fig. S7a, the sea level was very low and the top aquifer was largely unsaturated so the flow was dominated by vertical infiltration, and the topography-controlled lateral flow only presented in the freshwater areas of the basal aquifer. With time going by, the development of the surficial aquitard would enlarge the discharge limb (Zhang et al., 2022), and the lateral flow in the shallow aquifer gradually emerged, as shown in Figs. S7b to S7f. At the end of Holocene (Fig. S7f), there were two layers of typical lateral flow in the freshwater areas of shallow and basal aquifers after the surficial aquitard was completely formed. The flow in the saltwater areas of shallow and basal aquifers was primarily controlled by Haline convection.

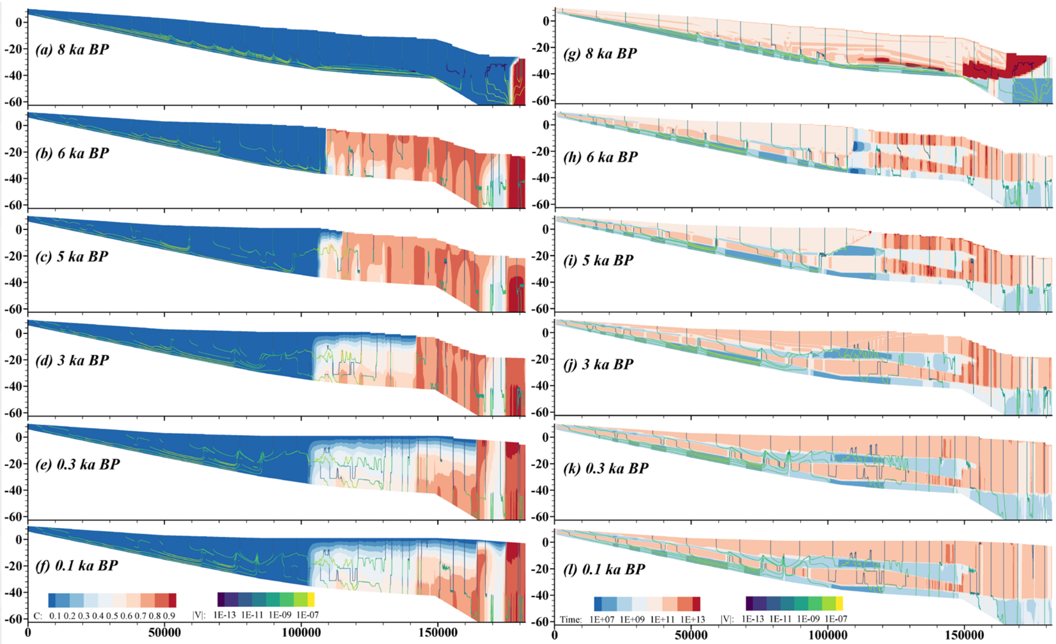


Figure S7. Evolutionary history of groundwater salinity distribution (a-f) and transit time distribution (g-l) in the Quaternary delta system during the Holocene. The velocity direction is denoted by the streamlines with velocity magnitude expressed in color bands. The salinity value is normalized as the salinity ratio of groundwater to seawater and the units of velocity and time are m/s and s, respectively.

During the Holocene, the $\delta^{18}O$ of the seawater, ranging from -0.8‰ to 2‰, was enriched by roughly 1‰ in comparison to the modern seawater (Morrissey et al., 2010; Sue, 2000). The isotope content of precipitation during the Holocene was very likely heavier than the modern record (-8~-4‰) along the subtropical coasts (Jasechko et al., 2015; Wang and Jiao, 2012). The groundwater in MZ near the sea had heavy $\delta^{18}O$ starting from the middle of the Holocene aquitard to the basal aquifer (Fig. S8c), suggesting that the enrichment can be attributed to the influence of Holocene seawater, which is also supported by the high TDS (Fig. S8j). A similar phenomenon occurred in HP from the middle of the shallow aquifer to the basal aquifer as well (Figs. S8b and S8i). The isotopic evidence supported the simulated results in the Quaternary delta system, which showed that the saline groundwater had been trapped in these areas such as HP and MZ for thousands of years (Figs. S7i-S7l). The stable isotope values of shallow groundwater samples in HP and MZ were close to the isotope content of modern rainfall (Wang and Jiao, 2012), indicating that modern precipitation serves as a freshwater recharge source in these areas. The trend towards $\delta^2H$ and $\delta^{18}O$ enrichment in freshwater samples in SD can be attributed to Holocene precipitation recharge and Holocene freshwater from inland sources. Based on the $\delta^{18}O$ and TDS values, the probable freshwater source is Holocene groundwater and precipitation (Figs. S8k and S8l).

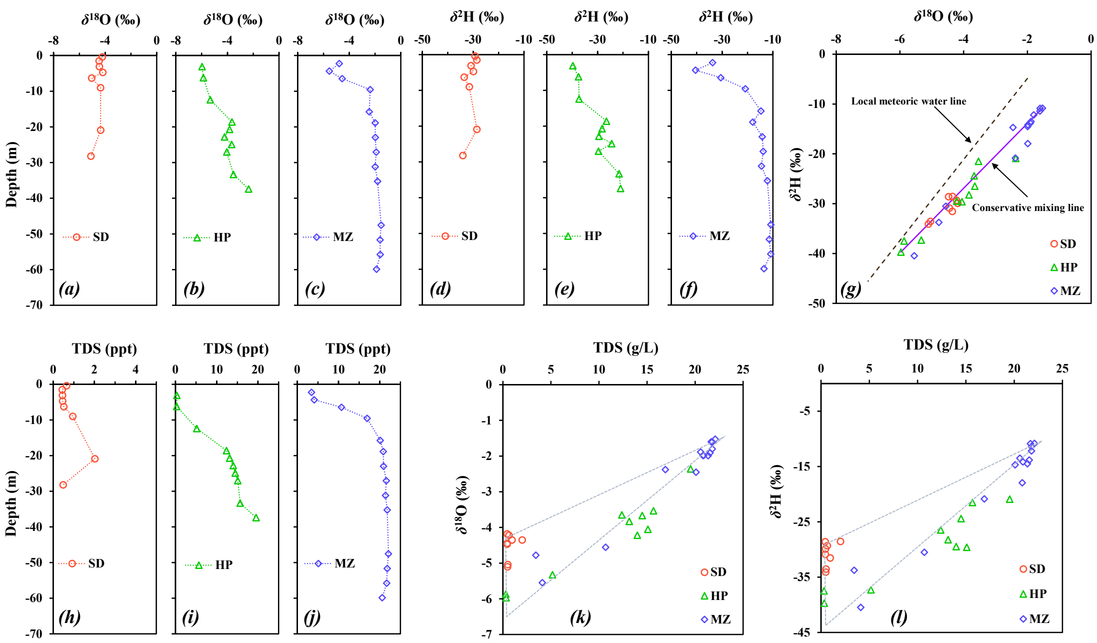


Figure S8. Stable isotope and total dissolved solid compositions of groundwater collected in multilevel sampling systems.

We calculated the total amount of salt mass in the delta system (Fig. S9a) to describe the evolution of the groundwater system during the Holocene. The seawater intrusion during transgression was the dominant input of salt. In the regressive period, the salt accumulation rates of different layers were both negative with low values (Fig. S9b), indicating that the continuous decline in salt mass happened but at a very slow speed. Although the salt amount experienced a decrease in the subsequent regression due to the flush of intruded saltwater, the newly developed marine sedimentary layer contained saltwater as well during the regressive phase. As a result, the total amount of salt changed little throughout the past 6000 years (Figs. S9a). The salt accumulation mainly occurred in the basal aquifer at the beginning of transgression and then moved to the Holocene aquitard. The shallow aquifer, meanwhile, possessed the least salt but with an apparent changing rate due to the rapid groundwater flow and short groundwater transit time (Figs. S7h-S7l). Although there was a gradual decline in the last three time slices (Fig. S9a), the percentage of salt in different layers only showed a slight change in the past 3000 years (Fig. S9c).

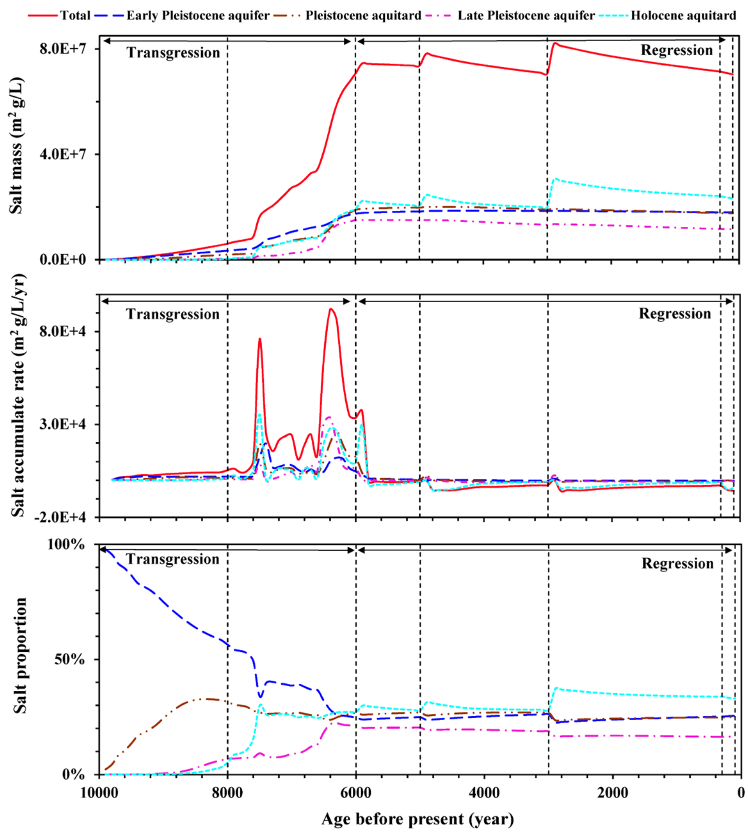


Figure S9. Changes of salt mass (a), salt accumulation rate (b), and salt proportion (c) in the Quaternary delta system.

The paleo groundwater discharge was dominated by the salt groundwater discharge which is also defined as the recirculated submarine groundwater discharge (Fig. S10). The paleo fresh groundwater discharge was impacted by the changing paleo precipitation, and its amount was nearly two orders of magnitude less than the total groundwater discharge or the salt groundwater discharge (Fig. S10), but it could be a potential source of existing offshore groundwater in the present-day sea (Post et al., 2013; Micallef et al., 2021).

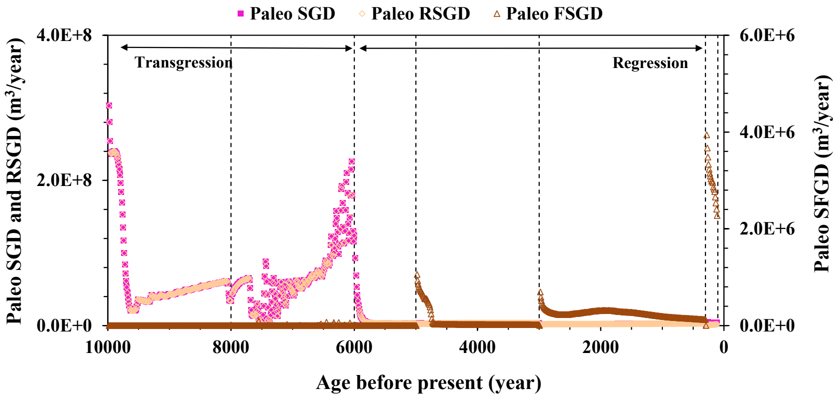


Figure S10. Groundwater discharge from the Quaternary delta system to the sea during the Holocene.

As far as the coastal deltaic aquifer system is concerned, precipitation provided fresh water to the system while seawater intrusion provided salt. The salinity inventory in the delta is mainly controlled by these two processes. The three indicators of water recharge, salt supply and mean annual change in salinity in the delta were employed to depict the dynamic process in the deltaic aquifer system, and their relationships can be seen in Fig. S11. The salinity inventory is positively correlated to both water recharge and salt supply. The sea level rise firstly caused a large volume of seawater into the delta, accompanied by the supply of salt (Fig. S11d). That is, the salinity inventory increased with the groundwater inventory when seawater intrusion was significant during the Holocene transgression (Figs. S11f-S11g). In the regressive period, the precipitation dominated the recharge and drove a small amount of groundwater to flow seaward (Figs. 3C-3F). The salinity inventory decreased as well because of the buffering effect of the deltaic aquifer system (Fig. 3I).

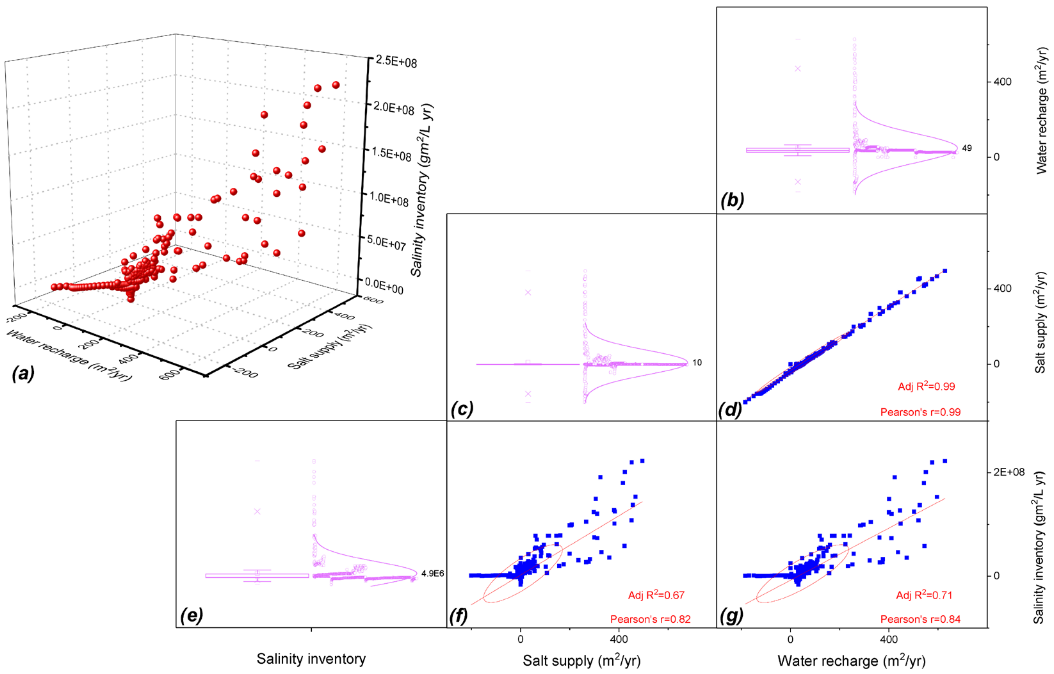


Figure S11. The relationships between water recharge, salt supply and salinity inventory in the delta.

## Limitations and future perspectives

In the PRD, surface water is mainly used for water supply due to extensive river network and abundant rainfall (Liu et al., 2018; Wang et al., 2016). Groundwater may be occasionally used by famers but overall its impact on groundwater flow system is very limited. As we mentioned before, the model covered the Holocene period of 10,000 years and we believe that the pumping from domestic wells in the past tens of years can be ignored in the model. Previous studies in the river-aquifer system of India and Nepal where the agricultural water demand is huge showed that the great pumping-induced reduction in dry-season baseflow would potentially affect downstream water users (Khan et al., 2022). In the circumstances, the lower course of a river will become salty when the discharge of the river is relatively small, and then the influence of salt tide on the regional groundwater flow systems should be considered.

Onshore saltwater and offshore freshwater, as two opposite geologic environments, have been observed in previous studies (Larsen et al., 2017; Micallef et al., 2020). We certainly found the offshore freshwater groundwater under the South China Sea, and results show that the observed offshore freshwater groundwater here was buried during the rapid transgressive period in the Holocene, while not formed due to the continuous flow of inland freshwater in the adjacent continental shelf. The reason why the model domain limited to the coast was that the coastal aquifers near the current sea level were full of seawater, and the density difference between inland freshwater and saltwater here stopped the freshwater from discharging into the seabed. We presumed that the thick Quaternary aquifer systems with leaching effect presented in the basal aquifer can be used to explore the link between onshore saltwater and offshore freshwater, e.g. the Red River delta plain (Larsen et al., 2017). In order to better calibrate our model using the limited inland borehole data and accurately describe the evolutionary history of the groundwater system in the PRD during the Holocene, we selected the current model domain cut off near the coast. Indeed, there is a lack of studies exploring the link between the hydrogeological models and sediment transport models especially around the active reaction zone of sediment-seawater interface. There are two main processes accounting for the changes in sediment pathways, including sediment transported along the coast by ocean currents and surge storms during high sea-level period, and fluvial transport into the basin by tributaries during low sea-level period (Steckler et al., 2007). Integrating these processes of sediment supply as a function of sea level can provide a realistic stratigraphic architecture both laterally and vertically, which is an interesting future direction for the hydrogeological model considering both groundwater flow and sediment accumulation.

## References

Abdullah, A.D., Gisen, J.I., van der Zaag, P., Savenije, H.H., Karim, U.F., Masih, I., and Popescu, I., 2016, Predicting the salt water intrusion in the Shatt al-Arab estuary using an analytical approach: Hydrology and earth system sciences, v. 20(10), p. 4031-4042, https://doi.org/10.5194/hess-20-4031-2016.

Addo, K.A., Nicholls, R.J., Codjoe, S.N.A., and Abu, M., 2018, A biophysical and socioeconomic review of the Volta delta, Ghana: Journal of Coastal Research, v. 34(5), p. 1216-1226, https://doi.org/10.2112/JCOASTRES-D-17-00129.1.

Afroza, R., Mazumder, Q.H., Jahan, C.S., Kazi, M.A.I., Ahsan, M.A., and Al-Mansur, M.A., 2009, Hydrochemistry and origin of salinity in groundwater in parts of lower Tista floodplain, Northwest Bangladesh: Journal of the Geological Society of India, v. 74(2), p. 223-232, https://doi.org/10.1007/s12594-009-0124-7.

Akouvi, A., Dray, M., Violette, S., de Marsily, G., and Zuppi, G.M., 2008, The sedimentary coastal basin of Togo: example of a multilayered aquifer still influenced by a palaeo-seawater intrusion: Hydrogeology journal, v. 16(3), p. 419-436, https://doi.org/10.1007/s10040-007-0246-1.

Albert, P., and Jorge, G., 1998, Coastal changes in the Ebro delta: Natural and human factors: Journal of Coastal Conservation, v. 4(1), p. 17-26, https://doi.org/10.1007/BF02806485.

Alcérreca-Huerta, J.C., Callejas-Jiménez, M.E., Carrillo, L., and Castillo, M.M., 2019, Dam implications on salt-water intrusion and land use within a tropical estuarine environment of the Gulf of Mexico: Science of The Total Environment, v. 652, p. 1102-1112, https://doi.org/10.1016/j.scitotenv.2018.10.288.

Al-Jawad, M.M., Nedawi, D.R., and Al-Manssory, F.Y., 2018, Studies on Salt Distribution in the Northern Part of Shatt al-Arab Waterway, Iraq.

Andrews, S.W., Gross, E.S., and Hutton, P.H., 2017, Modeling salt intrusion in the San Francisco Estuary prior to anthropogenic influence: Continental Shelf Research, v. 146, p. 58-81, https://doi.org/10.1016/j.csr.2017.07.010.

Baigún, C.R., Puig, A., Minotti, P.G., Kandus, P., Quintana, R., Vicari, R., Bo, R., Oldani, N.O., and Nestler, J.A., 2008, Resource use in the Parana River Delta (Argentina): moving away from an ecohydrological approach: Ecohydrology & Hydrobiology, v. 8(2-4), p. 245-262, https://doi.org/10.2478/v10104-009-0019-7.

Barbecot, F., Marlin, C., Gibert, E., and Dever, L., 2000, Hydrochemical and isotopic characterisation of the Bathonian and Bajocian coastal aquifer of the Caen area (northern France): Applied Geochemistry, v. 15(6), p. 791-805, https://doi.org/10.1016/S0883-2927(99)00088-8.

Barbiero, L., Cunnac, S., Mané, L., Laperrousaz, C., Hammecker, C., and Maeght, J. L., 2001, Salt distribution in the Senegal middle valley: Analysis of a saline structure on planned irrigation schemes from N'Galenka creek: Agricultural Water Management, v. 46(3), p. 201-213, https://doi.org/10.1016/S0378-3774(00)00088-3.

Bernardino, A.F., Mazzuco, A.C.A., Souza, F.M., Santos, T.M., Sanders, C.J., Massone, C.G., Costa, R.F., Silva, A.E.B., Ferreira, T.O., Nóbrega, G.N., and Silva, T.S., 2022. The novel mangrove environment and composition of the Amazon Delta: Current Biology, v. 32(16), p. 3636-3640, https://doi.org/10.1016/j.cub.2022.06.071.

Bethke, C.M. and Johnson, T.M., 2002, Paradox of groundwater age: correction. Geology, v. 30(4), p. 385-388, https://doi.org/10.1130/0091-7613(2002)030<0386:POGAC>2.0.CO;2.

Bethke, C.M. and Johnson, T.M., 2008, Groundwater age and groundwater age dating: Annual Review of Earth and Planetary Sciences, v. 36(1), p. 121-152, https://doi.org/10.1146/annurev.earth.36.031207.124210.

Bobba, A.G., 2002, Numerical modelling of salt-water intrusion due to human activities and sea-level change in the Godavari Delta, India: Hydrological Sciences Journal, v. 47(S1), p. S67-S80, https://doi.org/10.1080/02626660209493023.

Bolshiyanov, D., Makarov, A., and Savelieva, L., 2015, Lena River delta formation during the Holocene: Biogeosciences, v. 12(2), p. 579-593, https://doi.org/10.5194/bg-12-579-2015.

Bouillon, S., Dehairs, F., Schiettecatte, L.S., and Borges, A.V., 2007, Biogeochemistry of the Tana estuary and delta (northern Kenya): Limnology and Oceanography, v. 52(1), p. 46-59, https://doi.org/10.4319/lo.2007.52.1.0046.

Boyd, C.E., 2015, Water Quality: An Introduction. Springer.

Cao, Z., Dai, M., Zheng, N., Wang, D., Li, Q., Zhai, W., Meng, F., and Gan, J., 2011, Dynamics of the carbonate system in a large continental shelf system under the influence of both a river plume and coastal upwelling: Journal of Geophysical Research: Biogeosciences, v. 116(G2), https://doi.org/10.1029/2010JG001596.

Cardoso-Mohedano, J.G., Canales-Delgadillo, J.C., Machain-Castillo, M.L., Sanchez-Muñoz, W.N., Sanchez-Cabeza, J.A., Esqueda-Lara, K., Gómez-Ponce, M.A., Ruiz-Fernández, A.C., Alonso-Rodríguez, R., Lestayo-González, J.A., and Merino-Ibarra, M., 2022, Contrasting nutrient distributions during dry and rainy seasons in coastal waters of the southern Gulf of Mexico driven by the Grijalva-Usumacinta River discharges: Marine Pollution Bulletin, v. 178, p. 113584, https://doi.org/10.1016/j.marpolbul.2022.113584.

Cencini, C., 1998, Physical processes and human activities in the evolution of the Po delta, Italy: Journal of Coastal Research, p. 775-793, http://www.jstor.org/stable/4298834.

Collins, D. S., Johnson, H. D., and Baldwin, C.T., 2020, Architecture and preservation in the fluvial to marine transition zone of a mixed‐process humid‐tropical delta: Middle Miocene Lambir Formation, Baram Delta Province, north‐west Borneo: Sedimentology, v. 67(1), p. 1-46, https://doi.org/10.1111/sed.12622.

Dai, Z., Chu, A., Stive, M., Zhang, X., and Yan, H., 2011, Unusual salinity conditions in the Yangtze Estuary in 2006: Impacts of an extreme drought or of the Three Gorges Dam: Ambio, v. 40(5), p. 496-505, https://doi.org/10.1007/s13280-011-

0148-2.

Das Gupta, A., 1985, Simulated Salt-Water Movement in the Nakhon Luang Aquifer, Bangkok, Thailand: Groundwater, v. 23, (4), p. 512-522, https://doi.org/10.1111/j.1745-6584.1985.tb01501.x.

De Montety, V., Radakovitch, O., Vallet-Coulomb, C., Blavoux, B., and Travi, Y., 2005, Geochemical evolution and timescale of seawater intrusion in a confined coastal aquifer: Case of the Rhone delta. 13th IWRA World Water Congress, Montpellier, 1-4 Sept.

Delsman, J.R., Hu-A-Ng, K.R.M., Vos, P.C., De Louw, P.G., Oude Essink, G.H., Stuyfzand, P.J., and Bierkens, M.F., 2014, Paleo-modeling of coastal saltwater intrusion during the Holocene: an application to the Netherlands: Hydrology and Earth System Sciences, v. 18(10), p. 3891-3905, https://doi.org/10.5194/hess-18-3891-2014.

Devendra, D., Xiang, R. and Thilakanayaka, V., 2019, Paleoproductivity changes in the Southern South China Sea from the Last Glacial to the Holocene: Evidence from Stable Isotopes and Total Organic Carbon: International Journal of Geology and Earth Sciences, v. 5(2), p. 1-14, https://doi.org/10.18178/ijges.

Echezuría, H., Córdova, J., González, M., González, V., Méndez, J., and Yanes, C., 2002, Assessment of environmental changes in the Orinoco River delta: Regional Environmental Change, v. 3(1), p. 20-35, https://doi.org/10.1007/s10113-001-0038-4.

Eslami, S., Hoekstra, P., Kernkamp, H.W., Nguyen Trung, N., Do Duc, D., Nguyen Nghia, H., Tran Quang, T., Van Dam, A., Darby, S.E., Parsons, D.R., and Vasilopoulos, G., 2021, Dynamics of salt intrusion in the Mekong Delta: results of field observations and integrated coastal–inland modelling: Earth Surface Dynamics, v. 9(4), p. 953-976, https://doi.org/10.5194/esurf-9-953-2021.

Eslami, S., Hoekstra, P., Minderhoud, P.S., Trung, N.N., Hoch, J.M., Sutanudjaja, E.H., Dung, D.D., Tho, T.Q., Voepel, H.E., Woillez, M.N., and van der Vegt, M., 2021, Projections of salt intrusion in a mega-delta under climatic and anthropogenic stressors: Communications Earth & Environment, v. 2(1), p. 1-11, https://doi.org/10.1038/s43247-021-00208-5.

Geng, X. and Boufadel, M.C., 2015, Impacts of evaporation on subsurface flow and salt accumulation in a tidally influenced beach: Water Resources Research, v. 51(7), p. 5547-5565, https://doi.org/10.1002/2015WR016886.

Geriesh, M.H., Balke, K.D., El-Rayes, A.E., and Mansour, B.M., 2015, Implications of climate change on the groundwater flow regime and geochemistry of the Nile Delta, Egypt: Journal of coastal conservation, v. 19(4), p. 589-608, https://doi.org/10.1007/s11852-015-0409-5.

Giambastiani, B.M.S., Colombani, N., Mastrocicco, M., and Fidelibus, M.D., 2013, Characterization of the lowland coastal aquifer of Comacchio (Ferrara, Italy): hydrology, hydrochemistry and evolution of the system: Journal of Hydrology, v. 501, p. 35-44, https://doi.org/10.1016/j.jhydrol.2013.07.037.

Groen, J., Velstra, J., and Meesters, A.G.C.A., 2000, Salinization processes in paleowaters in coastal sediments of Suriname: evidence from δ37Cl analysis and diffusion modelling: Journal of Hydrology, v. 234(1-2), p. 1-20, https://doi.org/10.1016/S0022-1694(00)00235-3.

Haddout, S., Maslouhi, A., and Igouzal, M., 2017, Predicting of salt water intrusion in the Sebou river estuary (Morocco): Journal of Applied Water Engineering and Research, v. 5(1), p. 40-50, https://doi.org/10.1080/23249676.2015.1124029.

Harris, S. A., 1990, Dynamics and origin of saline soils on the Slims River delta, Kluane National Park, Yukon Territory: Arctic, p. 159-175, https://www.jstor.org/stable/40511142.

Jasechko, S., Lechler, A., Pausata, F.S., Fawcett, P.J., Gleeson, T., Cendón, D.I., Galewsky, J., LeGrande, A.N., Risi, C., Sharp, Z.D., and Welker, J.M., 2015, Late-glacial to late-Holocene shifts in global precipitation δ18O: Climate of the Past, v. 11(10), p. 1375-1393, https://doi.org/10.5194/cp-11-1375-2015.

Jiang, X.W., Wan, L., Ge, S., Cao, G.L., Hou, G.C., Hu, F.S., Wang, X.S., Li, H. and Liang, S.H., 2012, A quantitative study on accumulation of age mass around stagnation points in nested flow systems: Water Resources Research, v. 48(12), https://doi.org/10.1029/2012WR012509.

Kannan, R., Naidu, K. A., Kanungo, A., Murty, M. V., Avishek, K., and Ramana, K.V., 2022, Hydrochemical Characteristics of Groundwater—Assessment of Saltwater Intrusion Along Krishna and Godavari Delta Region, Andhra Pradesh, India. In Geospatial Technology for Landscape and Environmental Management Springer, Singapore, https://doi.org/10.1007/978-981-16-7373-3_5.

Kashef, A.A.I., 1983, Salt‐Water Intrusion in the Nile Delta: Groundwater, v. 21(2), p. 160-167, https://doi.org/10.1111/j.1745-6584.1983.tb00713.x.

Khan, M.R., Michael, H.A., Bresnyan, E.W. and Yu, W., 2022, Impacts of basin-wide irrigation pumping on dry-period stream baseflow in an alluvial aquifer in the

Kosi Fan region of India and Nepal: Hydrogeology Journal, v. 30(6), p. 1899-1910, https://doi.org/10.1007/s10040-022-02527-z.

Kipp, L.E., Henderson, P.B., Wang, Z.A., and Charette, M.A., 2020, Deltaic and estuarine controls on Mackenzie River solute fluxes to the Arctic Ocean: Estuaries and Coasts, v. 43(8), p. 1992-2014, https://doi.org/10.1007/s12237-020-00739-8.

Larsen, F., Tran, L.V., Van Hoang, H., Tran, L.T., Christiansen, A.V., and Pham, N.Q., 2017, Groundwater salinity influenced by Holocene seawater trapped in incised valleys in the Red River delta plain: Nature Geoscience, v. 10(5), p. 376-381, https://doi.org/10.1038/ngeo2938.

Lewis, E. and Wallace, D.W.R., 1998, Program Developed for CO2 System Calculations, ORNL/CDIAC-105, Carbon Dioxide Inf. Anal. Cent., Oak Ridge Natl. Lab.

Liu, B., Peng, S., Liao, Y. and Long, W., 2018, The causes and impacts of water resources crises in the Pearl River Delta: Journal of Cleaner Production, v. 177, p. 413-425, https://doi.org/10.1016/j.jclepro.2017.12.203.

Manzano, M., Custodio, E., Loosli, H., Cabrera, M.C., Riera, X., and Custodio, J., 2001, Palaeowater in coastal aquifers of Spain. Geological Society, London, Special Publications, v. 189(1), p. 107-138, https://doi.org/10.1144/GSL.SP.2001.189.01.08.

Mao, R., Luo, X., Jiao, J.J. and Li, H., 2023, Molecular diffusion and pore-scale mechanical dispersion controls on time-variant travel time distribution in hillslope aquifers: Journal of Hydrology, v. 616, p. 128798, https://doi.org/10.1016/j.jhydrol.2022.128798.

Micallef, A., Person, M., Haroon, A., Weymer, B.A., Jegen, M., Schwalenberg, K., Faghih, Z., Duan, S., Cohen, D., Mountjoy, J.J. and Woelz, S., 2020, 3D characterisation and quantification of an offshore freshened groundwater system in the Canterbury Bight: Nature communications, v. 11(1), p. 1-15, https://doi.org/10.1038/s41467-020-14770-7.

Micallef, A., Person, M., Berndt, C., Bertoni, C., Cohen, D., Dugan, B., Evans, R., Haroon, A., Hensen, C., Jegen, M., and Key, K., 2021, Offshore freshened groundwater in continental margins: Reviews of Geophysics, v. 59(1), p. e2020RG000706, https://doi.org/10.1029/2020RG000706.

Michael, H.A., Charette, M.A. and Harvey, C.F., 2011, Patterns and variability of groundwater flow and radium activity at the coast: A case study from Waquoit Bay, Massachusetts: Marine Chemistry, v. 127(1-4), p. 100-114, https://doi.org/10.1016/j.marchem.2011.08.001.

Morrissey, S.K., Clark, J.F., Bennett, M., Richardson, E., and Stute, M., 2010, Groundwater reorganization in the Floridan aquifer following Holocene sea-level rise: Nature Geoscience, v. 3(10), p. 683-687, https://doi.org/10.1038/ngeo956.

Mutia, D., Carpenter, S., Jacobs, Z., Jebri, F., Kamau, J., Kelly, S.J., Kimeli, A., Langat, P.K., Makori, A., Nencioli, F., and Painter, S.C., 2021, Productivity driven by Tana river discharge is spatially limited in Kenyan coastal waters: Ocean & Coastal Management, v. 211, p. 105713, https://doi.org/10.1016/j.ocecoaman.2021.105713.

Narayan, K.A., Schleeberger, C., & Bristow, K.L., 2007, Modelling seawater intrusion in the Burdekin Delta irrigation area, North Queensland, Australia: Agricultural Water Management, v. 89(3), p. 217-228, https://doi.org/10.1016/j.agwat.2007.01.008.

Naudts, L., Greinert, J., Artemov, Y., Staelens, P., Poort, J., Van Rensbergen, P., and De Batist, M., 2006, Geological and morphological setting of 2778 methane seeps in the Dnepr paleo-delta, northwestern Black Sea: Marine Geology, v. 227(3-4), p. 177-199, https://doi.org/10.1016/j.margeo.2005.10.005.

Oosterberg, W., Staras, M., Bogdan, L., Buijse, A.D., Constantinescu, A., Coops, H., Hanganu, J., Ibelings, B.W., Menting, G.A.M., Navodaru, I., and Török, L., 2000, Ecological gradients in the Danube Delta lakes: present state and man-induced changes.

Pellizzari, M., Naldi, M., Castaldelli, G., Ghion, F., Manfredini, E., Piccoli, F., and Viaroli, P., 2009, Salt and brackish lagoons of the Southern Po delta (Ferrara province, Emilia-Romagna region). Phytobenthos of the Italian Transitional Waters: Present Knowledge Status.

Post, V.E., Groen, J., Kooi, H., Person, M., Ge, S., and Edmunds, W.M., 2013, Offshore fresh groundwater reserves as a global phenomenon: Nature, v. 504(7478), p. 71-78, https://doi.org/10.1038/nature12858.

Post, V.E., Van der Plicht, H., and Meijer, H.A.J., 2003, The origin of brackish and saline groundwater in the coastal area of the Netherlands: Netherlands Journal of Geosciences, v. 82(2), p. 133-147, https://doi.org/10.1017/S0016774600020692.

Radhakrishna, I., 2001, Saline fresh water interface structure in Mahanadi delta region, Orissa, India: Environmental Geology, v. 40(3), p. 369-380, https://doi.org/10.1007/s002540000182.

Restrepo, J.C., Schrottke, K., Traini, C., Ortíz, J.C., Orejarena, A., Otero, L., Higgins, A., and Marriaga, L., 2016, Sediment transport and geomorphological change in a high-discharge tropical delta (Magdalena River, Colombia): Insights from a period of intense change and human intervention (1990–2010): Journal of Coastal Research, v. 32(3), p. 575-589, https://doi.org/10.2112/JCOASTRES-D-14-00263.1.

Rodolfo, K.S., 1975, The Irrawaddy Delta: tertiary setting and modern offshore sedimentation.

Samsudin, A.R., Haryono, A., Hamzah, U., and Rafek, A.G., 2008, Salinity mapping of coastal groundwater aquifers using hydrogeochemical and geophysical methods: a case study from north Kelantan, Malaysia: Environmental Geology, v. 55(8), p. 1737-1743, https://doi.org/10.1007/s00254-007-1124-9.

Shaghude, Y.W., 2005, Coastal Impacts of Water Abstraction and Impoundment in Africa: the Case of Rufiji River, http://hdl.handle.net/1834/187.

Sherin, V.R., Durand, F., Papa, F., Islam, A.S., Gopalakrishna, V.V., Khaki,M., and Suneel, V., 2020, Recent salinity intrusion in the Bengal delta: Observations and possible causes: Continental Shelf Research, v. 202, p. 104142, https://doi.org/10.1016/j.csr.2020.104142.

Shiller, A.M., and Boyle, E.A., 1991, Trace elements in the Mississippi River Delta outflow region: Behavior at high discharge: Geochimica et Cosmochimica Acta, v. 55(11), p. 3241-3251, https://doi.org/10.1016/0016-7037(91)90486-O.

Simpson, G., and Hutcheon, I., 1995, Pore-water chemistry and diagenesis of the modern Fraser River Delta: Journal of Sedimentary Research, v. 65(4a), p. 648-655, https://doi.org/10.1306/D426818A-2B26-11D7-8648000102C1865D.

Smith, S.V., Crossland, J.M., and Crossland, C.J., 1999, Mexican and central American coastal lagoon systems: carbon, nitrogen and phosphorus fluxes (regional workshop II). LOICZ International Project Office, Netherlands Institute for Sea Research.

Spiteri, C., Slomp, C.P., Charette, M.A., Tuncay, K. and Meile, C., 2008a, Flow and nutrient dynamics in a subterranean estuary (Waquoit Bay, MA, USA): field data and reactive transport modeling: Geochimica et Cosmochimica Acta, v. 72(14), p. 3398-3412, https://doi.org/10.1016/j.gca.2008.04.027.

Spiteri, C., Slomp, C.P., Tuncay, K., and Meile, C., 2008b, Modeling biogeochemical processes in subterranean estuaries: Effect of flow dynamics and redox conditions on submarine groundwater discharge of nutrients: Water Resources Research, v. 44(2), p. W02430, https://doi.org/10.1029/2007WR006071.

Spiteri, C., Van Cappellen, P. and Regnier, P., 2008c, Surface complexation effects on phosphate adsorption to ferric iron oxyhydroxides along pH and salinity gradients in estuaries and coastal aquifers: Geochimica et Cosmochimica Acta, v. 72(14), p. 3431-3445, https://doi.org/10.1016/j.gca.2008.05.003.

Storms, J.E., Hoogendoorn, R.M., Dam, R.A., Hoitink, A.J.F., and Kroonenberg, S.B., 2005, Late-holocene evolution of the Mahakam delta, East Kalimantan, Indonesia: Sedimentary Geology, v. 180(3-4), p. 149-166, https://doi.org/10.1016/j.sedgeo.2005.08.003.

Stovba, S.M., and Stephenson, R.A., 2002, Style and timing of salt tectonics in the Dniepr-Donets Basin (Ukraine): implications for triggering and driving mechanisms of salt movement in sedimentary basins: Marine and Petroleum Geology, v. 19(10), p. 1169-1189, https://doi.org/10.1016/S0264-8172(03)00023-0.

Su, R., Zhuang, Y., Sui, D., Xu, Y., Sun, L., Chen, H., Sun, D., Li, B. and Wang, F., 2014, Carbon isotopic records of middle Holocene corals and environmental causes in northern South China Sea: Quaternary International, v. 349, p. 257-269, https://doi.org/10.1016/j.quaint.2014.08.030.

Sue, F.H., 2000, Depth distributions of δ18O and Changes in mixed layer thickness in the South China Sea. National Sun Yat-Sen University, Master's thesis.

Terenzi, J., Jorgenson, M.T., Ely, C.R., and Giguère, N., 2014, Storm-surge flooding on the Yukon-Kuskokwim delta, Alaska: Arctic, p. 360-374, https://www.jstor.org/stable/24363780.

Törnqvist, T.E., Jankowski, K.L., Li, Y.X., and González, J.L., 2020, Tipping points of Mississippi Delta marshes due to accelerated sea-level rise: Science Advances, v. 6(21), p. eaaz5512, https://www.science.org/doi/10.1126/sciadv.aaz5512.

Tran, L.T., Larsen, F., Pham, N.Q., Christiansen, A.V., Tran, N., Vu, H.V., Tran, L.V., Hoang, H.V., and Hinsby, K., 2012, Origin and extent of fresh groundwater, salty paleowaters and recent saltwater intrusions in Red River flood plain aquifers, Vietnam: Hydrogeology journal, v. 20(7), p. 1295-1313, https://doi.org/10.1007/s10040-012-0874-y.

Waelbroeck, C., Labeyrie, L., Michel, E., Duplessy, J.C., Mcmanus, J.F., Lambeck, K., Balbon, E. and Labracherie, M., 2002, Sea-level and deep water temperature changes derived from benthic foraminifera isotopic records: Quaternary Science Reviews, v. 21(1-3), p. 295-305, https://doi.org/10.1016/S0277-3791(01)00101-9.

Wang, Y., and Jiao, J.J., 2012, Origin of groundwater salinity and hydrogeochemical processes in the confined Quaternary aquifer of the Pearl River Delta, China: Journal of Hydrology, v. 438, p. 112-124, https://doi.org/10.1016/j.jhydrol.2012.03.008.

Wang, Z., Liu, Y., Li, Y., Zhao, P. and Yu, J., 2016, Legislation on protection of drinking water sources and local management practices in the Pearl River Delta region of China: Chinese Journal of Population Resources and Environment, v. 14(2), p. 144-152, https://doi.org/10.1080/10042857.2015.1113651.

Witcher, J.C., King, J.P., Hawley, J.W., Kennedy, J.F., Williams, J., Cleary, M., and Bothern, L.R., 2004, Sources of salinity in the Rio Grande and Mesilla Basin groundwater. New Mexico Water Resources Research Institute Technical Completion Report, v. 330, p. 168.

Xie, Y., Love, A.J., Simmons, C.T., Costar, A. and Wu, J., 2022, Groundwater age persistence in topography-driven groundwater flow over paleohydrogeologic time scales: Geology, v. 50(6), p. 731-735, https://doi.org/10.1130/G49842.1.

Yu, J., Li, Y., Han, G., Zhou, D., Fu, Y., Guan, B., Wang, G., Ning, K., Wu, H., and Wang, J., 2014, The spatial distribution characteristics of soil salinity in coastal zone of the Yellow River Delta: Environmental Earth Sciences, v. 72(2), p. 589-599, https://doi.org/10.1007/s12665-013-2980-0.

Zhang, H., Liu, C., Jin, X., Shi, J., Zhao, S. and Jian, Z., 2016, Dynamics of primary productivity in the northern South China Sea over the past 24,000 years: Geochemistry, Geophysics, Geosystems, v. 17(12), p. 4878-4891, https://doi.org/10.1002/2016GC006602.

Zhang, M., Wang, H., Pang, X., Liu, H., and Wang, Q., 2017, Characteristics of soil salinity in the typical area of Yellow River Delta and its control measures. In IOP Conference Series: Earth and Environmental Science, v. 64(1), p. 012078, https://doi.org/10.1088/1755-1315/64/1/012078.

Zong, Y., 2004, Mid-Holocene sea-level highstand along the Southeast Coast of China: Quaternary International, v. 117(1), p. 55-67, https://doi.org/10.1016/S1040-6182(03)00116-2.

Zong, Y., Huang, G., Switzer, A.D., Yu, F., and Yim, W.S., 2009a, An evolutionary model for the Holocene formation of the Pearl River delta, China: The Holocene, v. 19(1), p. 129-142, https://doi.org/10.1177/0959683608098957.

Zong, Y., Kemp, A.C., Yu, F., Lloyd, J.M., Huang, G., and Yim, W.W.S., 2010a, Diatoms from the Pearl River estuary, China and their suitability as water salinity indicators for coastal environments: Marine Micropaleontology, v. 75(1-4), p.

38-49, https://doi.org/10.1016/j.marmicro.2010.02.004.
Zong, Y., Lloyd, J.M., Leng, M.J., Yim, W.S., and Huang, G., 2006, Reconstruction of Holocene monsoon history from the Pearl River Estuary, southern China, using diatoms and carbon isotope ratios: The Holocene, v. 16(2), p. 251-263, https://doi.org/10.1191/0959683606hl911rp.
Zong, Y., Yim, W.S., Yu, F., and Huang, G., 2009b, Late Quaternary environmental changes in the Pearl River mouth region, China: Quaternary International, v. 206(1-2), p. 35-45, https://doi.org/10.1016/j.quaint.2008.10.012.
Zong, Y., Yu, F., Huang, G., Lloyd, J.M., and Yim, W.W.S., 2010b, The history of water salinity in the Pearl River estuary, China, during the Late Quaternary. Earth Surface Processes and Landforms, v. 35(10), p. 1221-1233, https://doi.org/10.1002/esp.2030.